GROUND DATA PROCESSING & PRODUCTION OF THE LEVEL 1 HIGH RESOLUTION MAPS

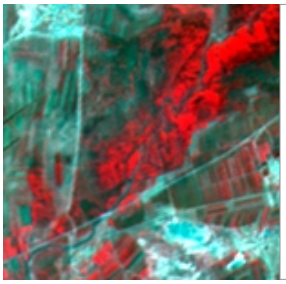

VALERI 2002

Zhang Bei site
(pastures)

Philippe Rossello

May 2008

CONTENTS

1. Introduction

This report describes the production of high resolution, level 1, biophysical variable maps for the Zhang Bei site in August 2002. Level 1 map corresponds to the map derived from the determination of a transfer function between reflectance values of the SPOT image acquired during (or around) the ground campaign, and biophysical variable measurements (hemispherical images). For each Elementary Sampling Unit (ESU), the hemispherical images were processed using the CAN-EYE software (Version 5) developed at INRA-EMMAH. The derived biophysical variable maps are:

• four Leaf Area Index (LAI) are considered: effective LAI (LAIeff) and true LAI (LAItrue) derived from the measurement of the gap fraction as a function of the view zenith angle; effective LAI57 (LAI57eff) and true LAI57 (LAI57true) derived from the gap fraction at 57.5°, which is independent on leaf inclination. Effective LAI and effective LAI57 do not take into account clumping effect. LAItrue and LAI57true are derived using the method proposed by Lang and Xiang[1] (1986);

• cover fraction (fCover): it is the percentage of soil covered by vegetation. To improve the spatial sampling, fCover was computed over 0 to 10° zenith angle;

• fAPAR: it is the fraction of Absorbed Photosynthetically Active Radiation (PAR = 400-700nm). CAN-EYE software proposes three outputs for fAPAR. Here, the selected output is the instantaneous 'black sky' fAPAR ($fAPAR^{BS}$): it is the black sky fAPAR at a given solar position (date, hour and latitude). Depending on latitude, CAN-EYE computes the solar zenith angle every solar hour during half the day (there is symmetry at 12:00). The instantaneous fAPAR is then approximated at each solar hour as the gap fraction in the corresponding solar zenith angle: $fAPAR^{BS}(\theta_s) = P_o(\theta_s)$.

For more information, you could read the following document: "CAN-EYE Output Variables. Definitions and theoretical background" (http://www.avignon.inra.fr/can_eye/Variables_Meaning_CAN_EYE.pdf).

The Zhang Bei site is mainly composed of pastures (for more information, see annex or campaign report: http://www.avignon.inra.fr/valeri). This flat area is 3 x 3 km with coordinates described in Table 1:

	UTM 50 North, WGS-84 (units = meters)		Geographic Lat/Lon WGS-84 (units = degrees)	
	Easting	Northing	Lat.	Lon.
Upper left corner	304833.9189	4573788.2170	41.29195659	114.66916764
Lower right corner	307873.9189	4570768.2170	41.26550409	114.70639798
Center	306353.9192	4572278.2172	41.27873196	114.68778657

Table 1. Description of the site coordinates.

The ground measurements were carried out from 8th to 10th August 2002 and the high spatial resolution image (SPOT2, HRV1, resolution: 20 m) was acquired fourteen days later.

2. Available data

2.1. SPOT Image

The SPOT image was acquired on 23rd August 2002 by HRV1 on SPOT2. It was geo-located by INRA. The projection is UTM 50 North, WGS-84. No atmospheric correction was applied to the image since no atmospheric data were available. However, as the SPOT image is used to compute empirical relationships between reflectance and biophysical variable, we can assume that the effect of the atmosphere is the same over the whole 3 x 3 km site. Therefore, it will be taken into account everywhere in the same way.

Figure 1 shows the relationship between Red and near infrared (NIR) SPOT channels: the soil line is marked and no saturated points are observed.

[1] Lang, A.R.G. and Xiang, Y., 1986. Estimation of leaf area index from transmission of direct sunlight in discontinuous canopies. Agric. For. Meteorol., 37: 229-243.

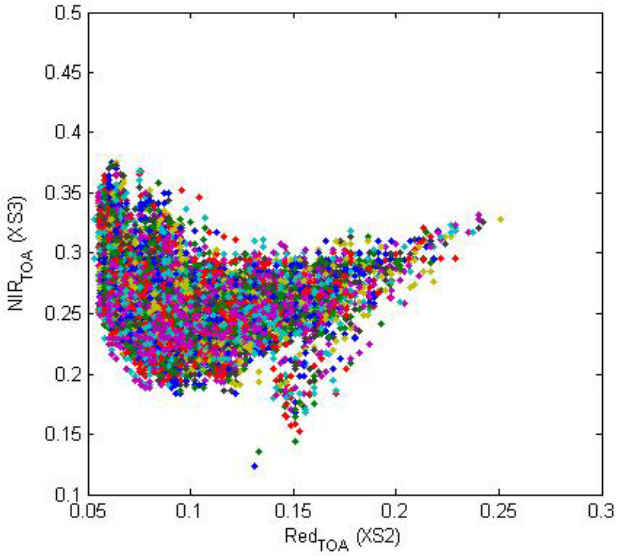

Figure 1. Red/NIR relationship on the SPOT image for Zhang Bei, 2002.

2.2. Hemispherical images

The hemispherical images were processed using the CAN-EYE software (Version 5) to derive the biophysical variables. Figure 2 and Figure 3 show the distribution of the several variables over the 47 sampled ESUs. In the VALERI context, the hemispherical images are acquired from above the understorey and from below the canopy (trees). The two sets of acquisition are processed separately to derive LAI (effective and true), LAI57 (effective and true), fCover, and fAPAR. The ESU biophysical variable is then computed as:

- LAIeff, LAI57eff, LAItrue, LAI57true: LAI(above) + LAI(below).
- fCover: 1-(1-fCover(above))*(1-fCover(below)). This assumes independency between the gaps inside the understorey and those inside the trees which is not true at all the scales but it is the only way to get the total fCover. However, for the local scales considered, this might be true as a first order approximation.
- fAPAR: 1-(1-fAPAR(below))*(1-fAPAR(above)), since 1-fAPAR can be considered equivalent to a gap fraction. Here again, the same independency between the two layers has to be assumed.

However, as the Zhang Bei site is mainly covered of pastures, the hemispherical images were only acquired from above the understorey.

Note that LAI (effective and true) derived from directional gap fraction and LAI derived from gap fraction at 57.5° (effective and true) are consistent (Figure 2 and Figure 3). Effective LAI (LAIeff, LAI57eff) varies from 0.24 to 2.43, while true LAI (LAItrue, LAI57true) varies from 0.26 to 2.93. The site is thus heterogeneous in terms of LAI (Figure 2). LAIeff and LAI57eff are lower than LAItrue and LAI57true, due to the clumping observed for several ESUs. The relationship between fAPAR and LAI is in agreement with what is expected (Beer-Lambert law) while the fCover-LAI relationship is more noisy (Figure 3).

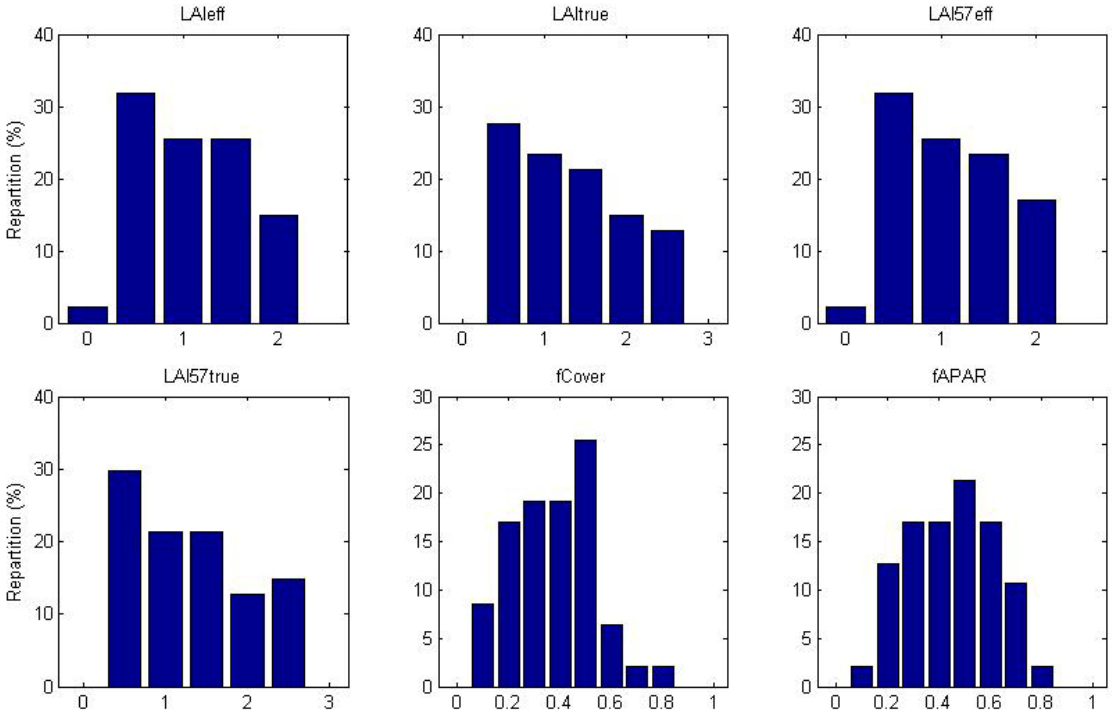

Figure 2. Distribution of the measured biophysical variables over the ESUs.

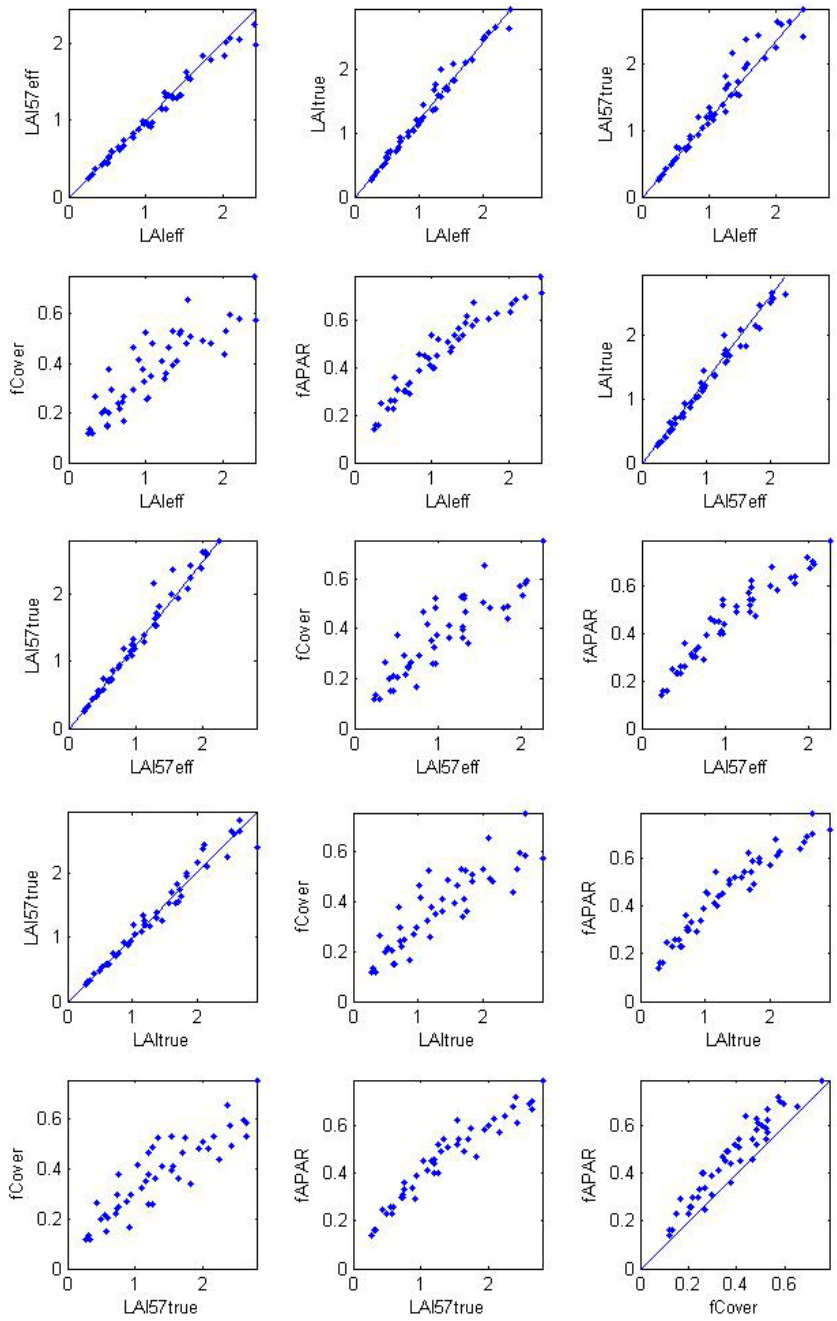

Figure 3. Relationships between the different biophysical variables.

2.3. Sampling strategy

2.3.1. Principles

Figure 4 shows that the 47 ESUs are evenly distributed over the site (3 x 3 km). Considering that SPOT geo-location and GPS measurements are associated to errors, we found that:

- A03, A12, B15 and B19 were located close to the road or the river: they have been shifted by 1 or 2 pixels.
- LAI for A09 did not correspond to the SPOT pixel in terms of reflectance as compared to the knowledge of the land use: it has been shifted by 1 pixel.

Finally, 47 ESUs have been kept for the computation of the transfer function.

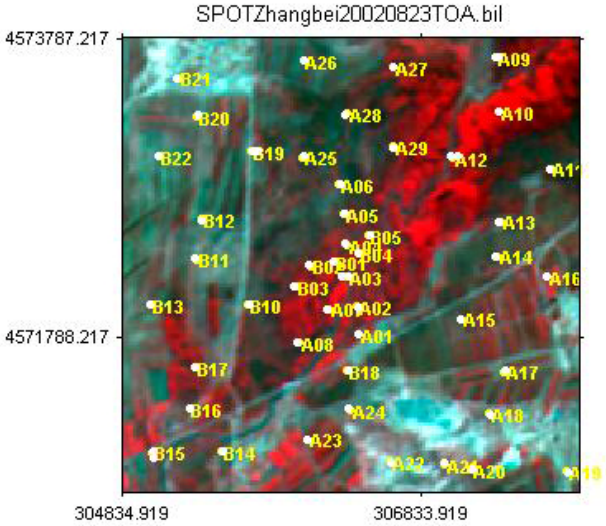

Figure 4. Distribution of the ESUs around the Zhang Bei site.

2.3.2. Evaluation based on NDVI values

The sampling strategy is evaluated using the SPOT image by comparing the NDVI distribution over the site with the NDVI distribution over the ESUs (Figure 5). As the number of pixels is drastically different for the ESUs and whole site (WS = 22500 in case of a 3 x 3 km SPOT image, resolution 20m), it is not statistically consistent to directly compare the two NDVI histograms. Therefore, the proposed technique consists in comparing the NDVI cumulative frequency of the two distributions by a Monte-Carlo procedure which aims at comparing the actual frequency to randomly shifted sampling patterns. It consists in:

1. computing the cumulative frequency of the *N* pixel NDVI that correspond to the exact ESU locations;
2. then, applying a unique random translation to the sampling design (modulo the size of the image);
3. computing the cumulative frequency of NDVI on the randomly shifted sampling design;
4. repeating steps 2 and 3, 199 times with 199 different random translation vectors.

This provides a total population of $N = 199 + 1$(actual) cumulative frequency on which a statistical test at acceptance probability $1 - \alpha = 95\%$ is applied: for a given NDVI level, if the actual ESU density function is between two limits defined by the $N\alpha/2 = 5$ highest and lowest values of the 200 cumulative frequencies, the hypothesis assuming that WS and ESU NDVI distributions are equivalent is accepted, otherwise it is rejected.

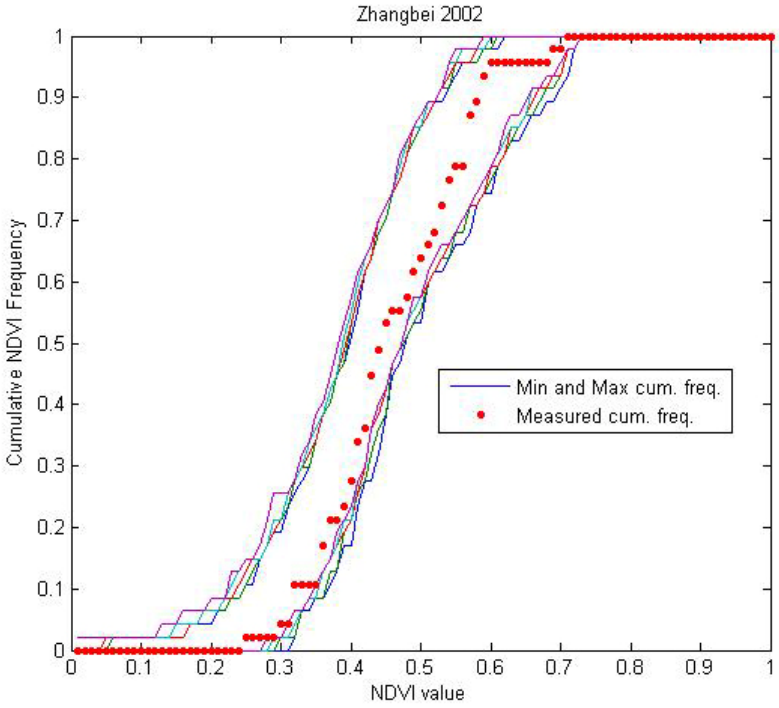

Figure 5. Comparison of the ESU NDVI distribution and the NDVI distribution over the whole image.

Figure 5 shows that the NDVI distribution of the 47 ESUs is good over the whole site (comprised between the 5 highest and lowest cumulative frequencies), even if the cumulative frequency curve is sometimes close to the boundaries (mainly for NDVI values comprised between 0.27 and 0.40). Note that NDVIs lower than 0.25 comprised between 0.26 and 0.29, between 0.33 and 0.35, between 0.61 and 0.68, have not been sampled although they are present in the image.

2.3.3. Evaluation based on classification

A non supervised classification based on the k_means method (Matlab statistics toolbox) was applied to the 3 reflectances of the SPOT image to distinguish if different behaviours on the image for the biophysical variable-reflectance relationship exist.

A number of 5 classes was chosen (Figure 6). The distribution of the classes on the image and on the ESUs is rather similar. Note that classes 2, 3 and 5 are under-represented and classes 1 and 4 appear to be over-sampled. Class 5 mainly corresponds to bare soil, villages…

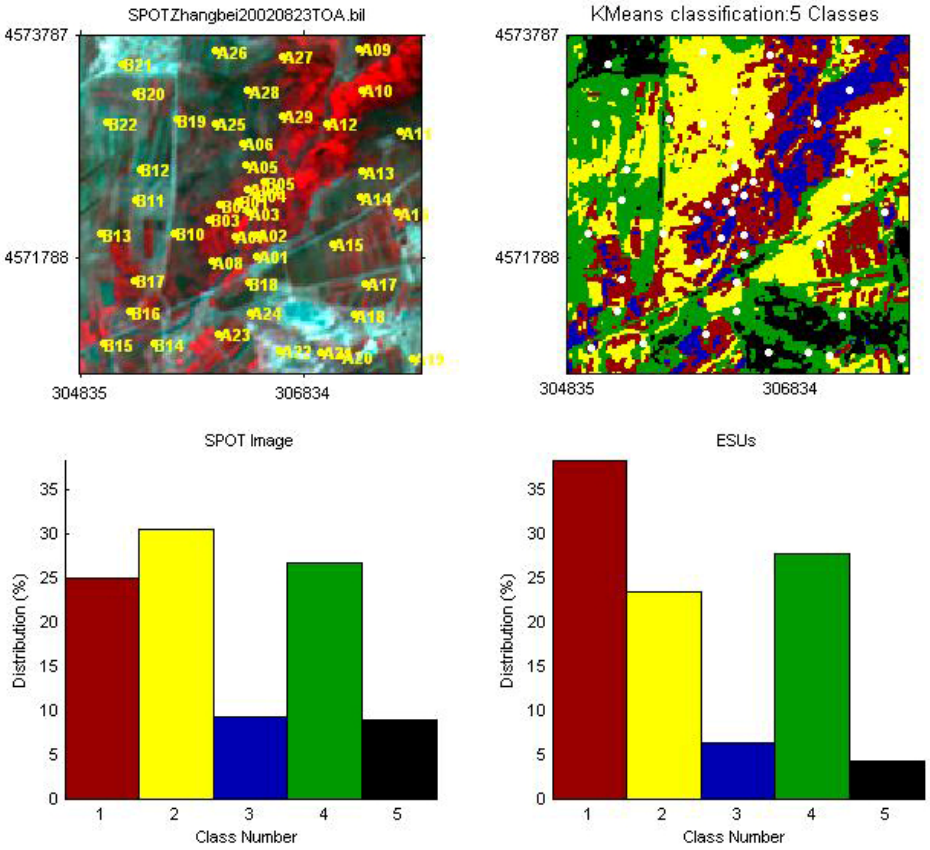

Figure 6. Classification of the SPOT image. Comparison of the class distribution between the SPOT image and sampled ESUs.

Figure 7 shows the different relationships observed between the biophysical variables and the corresponding NDVI on the ESUs, as a function of the SPOT classes determined from non supervised classification.

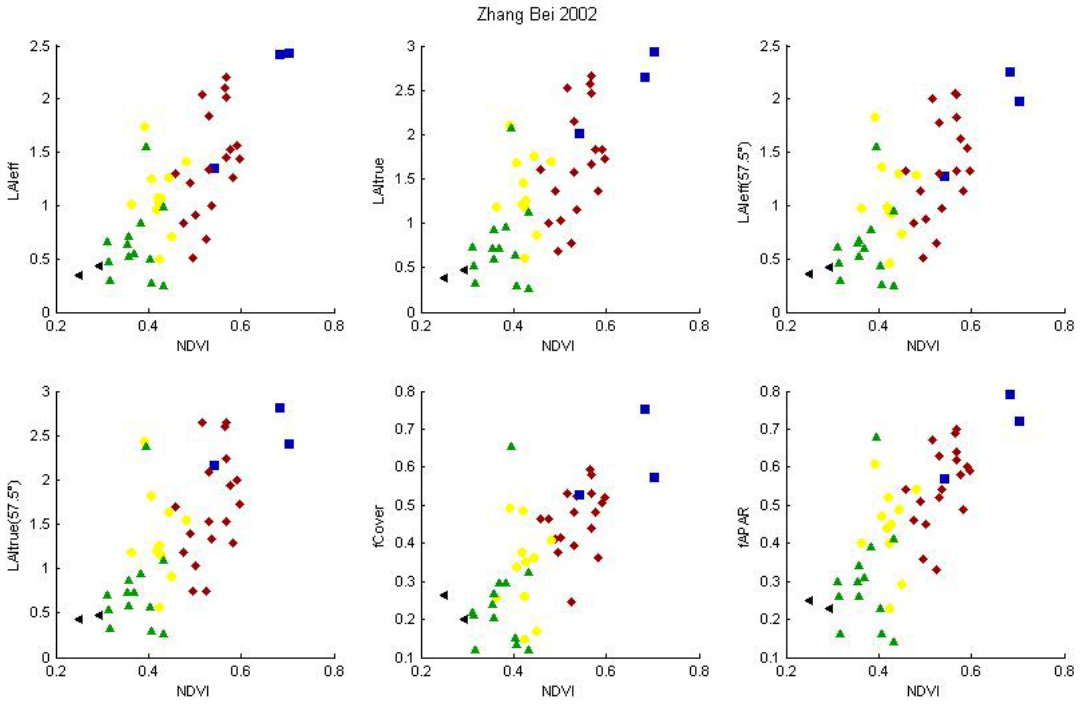

Figure 7. NDVI-Biophysical Variable relationships as a function of SPOT classes

The relation between NDVI and biophysical variables is consistent. Note that class 5 (villages, bare soil…) is represented by two ESUs (A22 and B21).

2.3.4. Using convex hulls

A test based on the convex hulls was also carried out to characterize the representativeness of ESUs. Whereas the evaluation based on NDVI values uses two bands (red and NIR), this test uses the three bands of the SPOT image. A flag image, is computing over the reflectances (Figure 8). The result on convex-hulls can be interpreted as:

- pixels inside the 'strict convex-hull': a convex-hull is computed using all the SPOT reflectance corresponding to the ESUs belonging to the class. These pixels are well represented by the ground sampling and therefore, when applying a transfer function the degree of confidence in the results will be quite high, since the transfer function will be used as an interpolator;
- pixels inside the 'large convex-hull': a convex-hull is computed using all the reflectance combination (±5% in relative value) corresponding to the ESUs. For these pixels, the degree of confidence in the obtained results will be quite good, since the transfer function is used as an extrapolator (but not far from interpolator);
- pixels outside the two convex-hulls: this means that for these pixels, the transfer function will behave as an extrapolator which makes the results less reliable. However, having a priori information on the site may help to evaluate the extrapolation capacities of the transfer function.

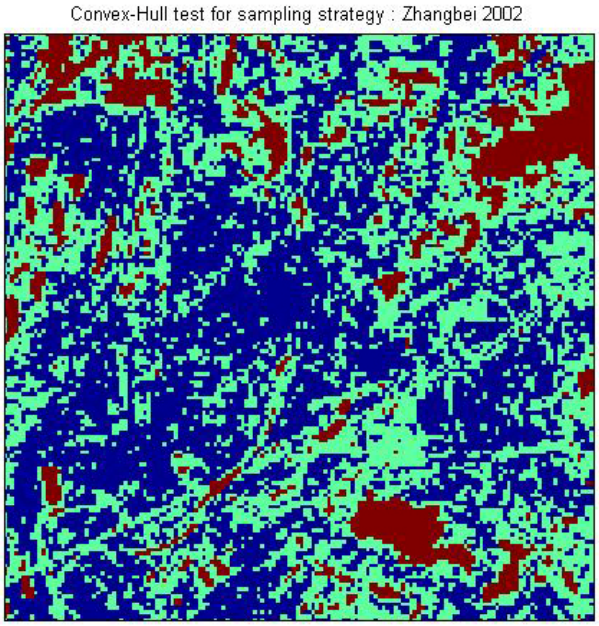

Figure 8. Evaluation of the sampling based on the convex hulls. The map is shown: blue and light blue correspond to the pixels belonging to the 'strict' and 'large' convex hulls and red to the pixels for which the transfer function is extrapolating.

This map shows that the representativeness of the ESUs is quite good, even if pixels are outside the two convex-hulls. They mainly correspond to low NDVI values (bare soil, villages…) and high NDVI values.

3. Determination of the transfer function for the 6 biophysical variables: LAIeff, LAItrue, LAI57eff, LAI57true, fCover, fAPAR

3.1. The transfer functions considered

Two types of transfer functions are usually tested in the frame of the VALERI project:

- AVE: if the number of ESUs belonging to the class is too low. The transfer function consists only in attributing the average value of the biophysical variable measured on the class to each pixel of the SPOT image belonging to the class;

- REG: if the number of ESUs is sufficient, multiple robust regression between ESUs reflectance (or Simple Ratio) and the considered biophysical variable can be applied: we used the 'robustfit' function from the matlab statistics toolbox. It uses an iteratively re-weighted least squares algorithm, with the weights at each iteration computed by applying the bisquare function to the residuals from the previous iteration. This algorithm provides lower weight to ESUs that do not fit well. The results are less sensitive to outliers in the data as compared with ordinary least squares regression. At the end of the processing, three errors are computed: classical root mean square error (RMSE), weighted RMSE (using the weights attributed to each ESU) and cross-validation RMSE (leave-one-out method).

The relationship between NDVI and LAI (§2.3.3) being consistent, the 'REG' method is applied to all the classes, even if two ESUs (A22, B21) characterize the class 5.

The 'REG' function is tested using either the reflectance or the logarithm of the reflectance for any band combination as well as the simple ratio or NDVI. As the method has poor extrapolation capacities, a flag image, based on the convex hulls is computing over reflectances.

3.2. Results

3.2.1. Choice of the method

A single transfer function was thus computed for all the classes. Figure 9 shows the results obtained for all the possible band combinations using either the reflectance (ρ) or the logarithm of the reflectance (log(ρ)). Even

if the regression made on the log(ρ) sometimes provides slightly better results, the results using the reflectance (ρ) were selected for all the variables. The transfer function using the log(ρ) indeed provides very high biophysical variable values.

Note that the Red*NIR ('+' or RN) combination is added to all the band combinations (except for NDVI and SR). Please read the document: "a method to improve the relation between the biophysical variables" (http://www.avignon.inra.fr/valeri/table_methods/new_linear.pdf).

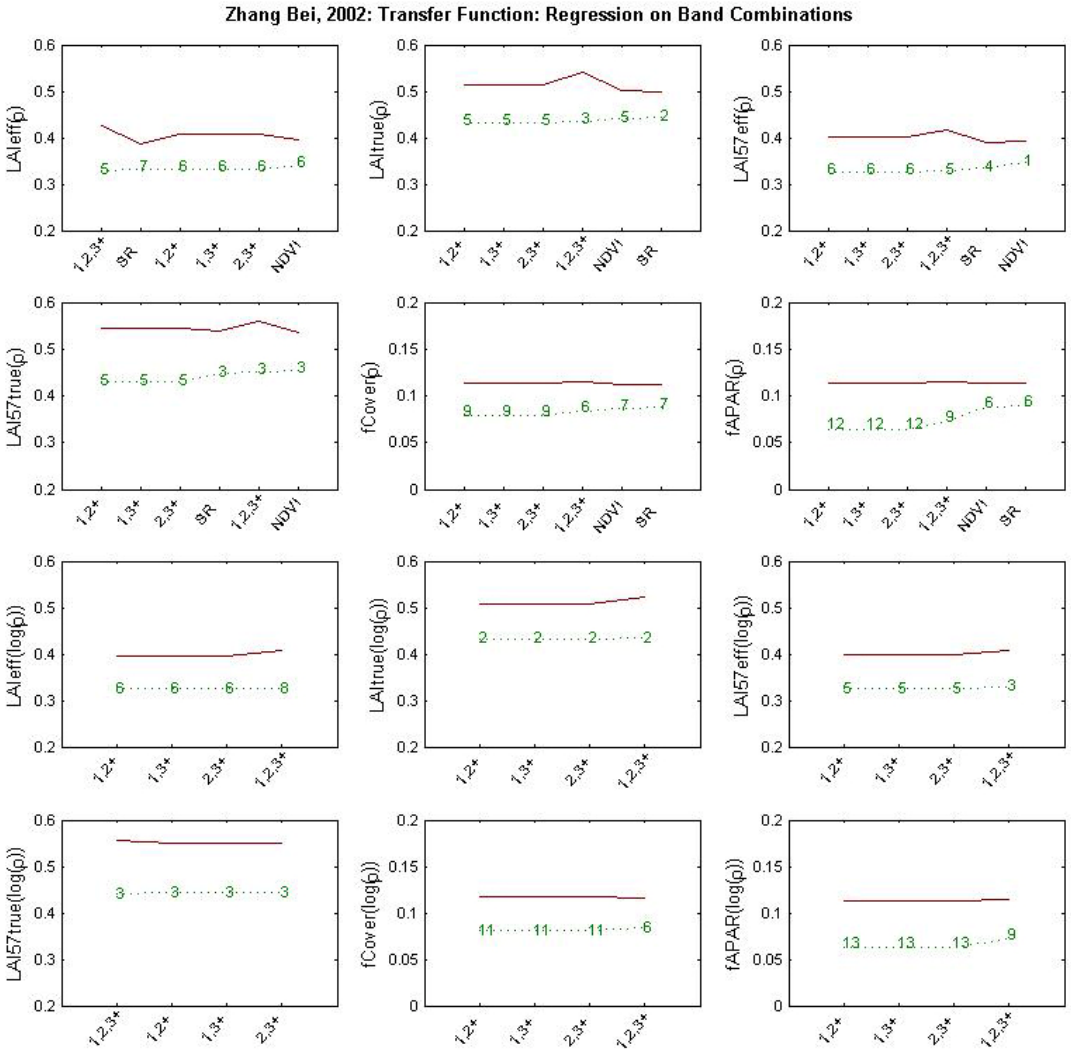

Figure 9. Transfer function: test of multiple regression applied on different band combinations. Band combinations are given in abscissa. The estimated biophysical variable is given in ordinate. Top graphs correspond to regression made on reflectance (ρ): the weighted root mean square error (RMSE) is presented in green along with the cross-validation RMSE in red. The numbers indicate the number of data used for the robust regression with a weight lower than 0.7 that could be considered as outliers. Bottom graphs correspond to regression made on the logarithm of the reflectance.

3.2.2. Choice of the band combination

For the LAIeff, the XS2, XS3, RN combination on reflectance (Figure 10 and Figure 11) was selected since it provides a good compromise between the cross-validation RMSE, the weighted RMSE and the RMSE. Note that six weights are lower than 0.7.

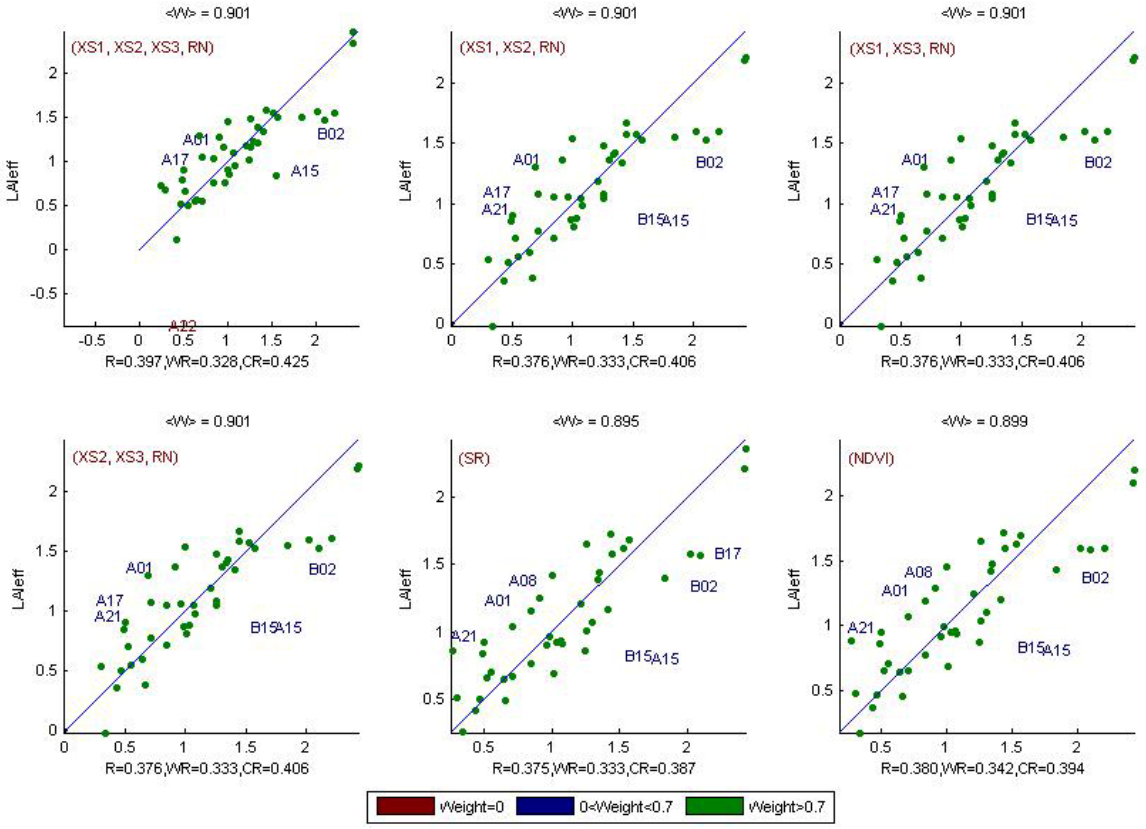

Figure 10. Effective Leaf Area Index: results for regression on reflectance using different band combinations. R is the root mean square error computed between LAIeff and estimated LAIeff. WR is the weighted root mean square error and CR is the cross validation root mean square error.

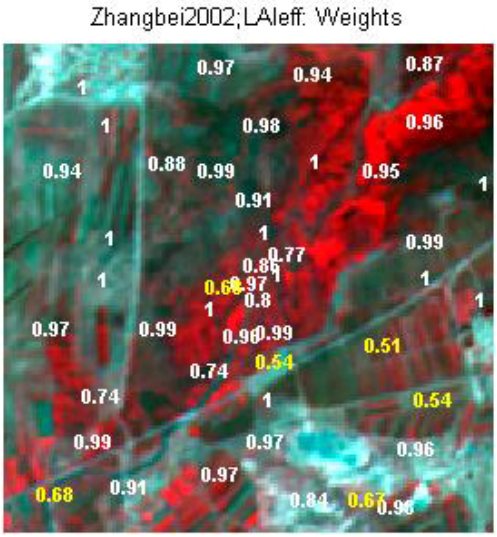

Figure 11. Weights associated to each ESU for the determination of LAIeff transfer function.

For the LAItrue, the XS2, XS3, RN combination on reflectance (Figure 12 and Figure 13) was selected since it provides a good compromise between the cross-validation RMSE, the weighted RMSE and the RMSE. Five weights are lower than 0.7. Note that the SR combination provides unrealistic results.

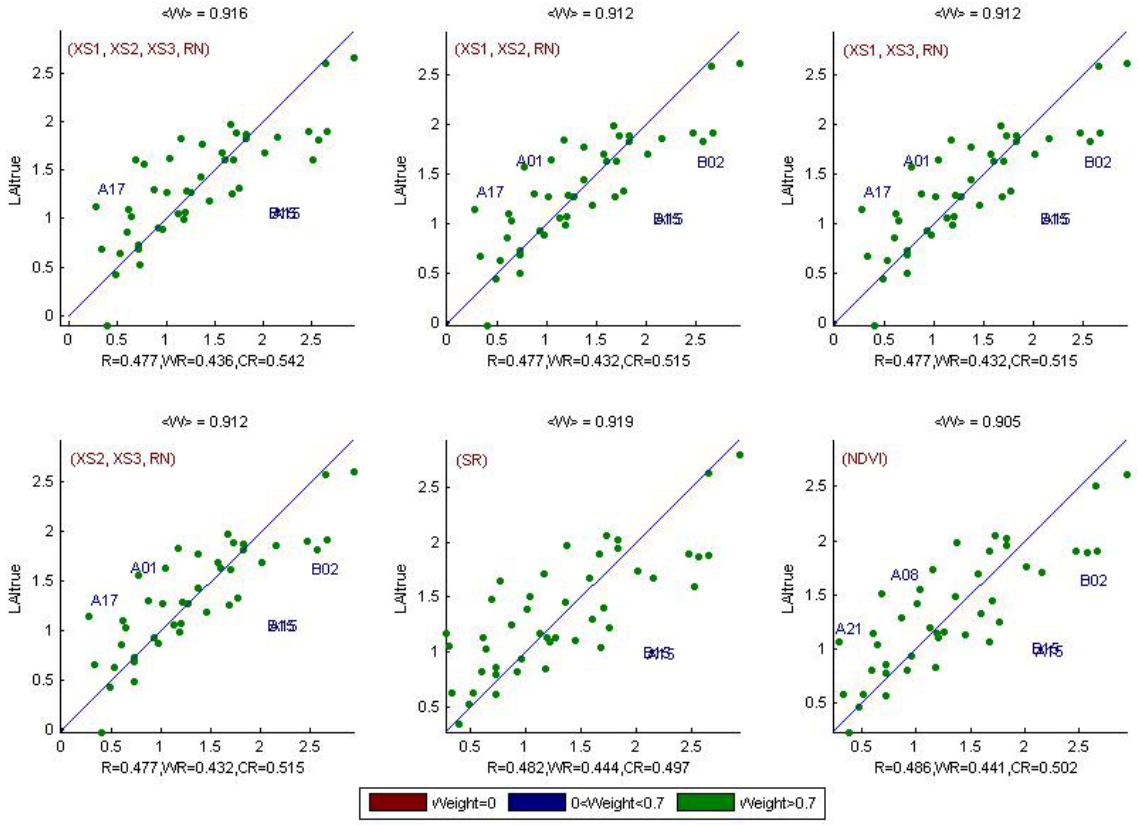

Figure 12. True Leaf Area Index: results for regression on reflectance using different band combinations. R is the root mean square error computed between LAItrue and estimated LAItrue. WR is the weighted root mean square error and CR is the cross validation root mean square error.

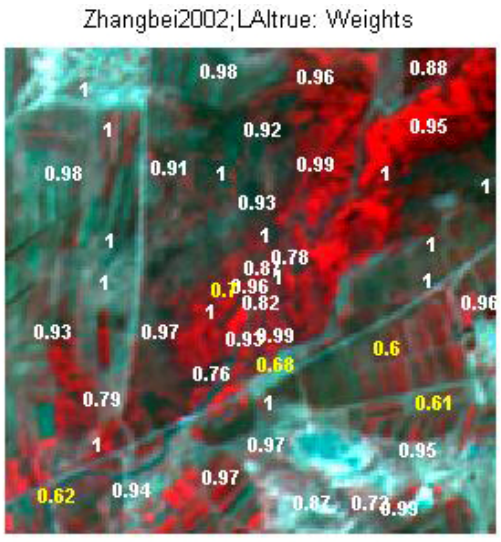

Figure 13. Weights associated to each ESU for the determination of LAItrue transfer function.

For the LAI57eff, the NDVI combination on reflectance (Figure 14 and Figure 15) was selected since it provides a good compromise between the cross-validation RMSE, the weighted RMSE and the RMSE. One weight is lower than 0.7.

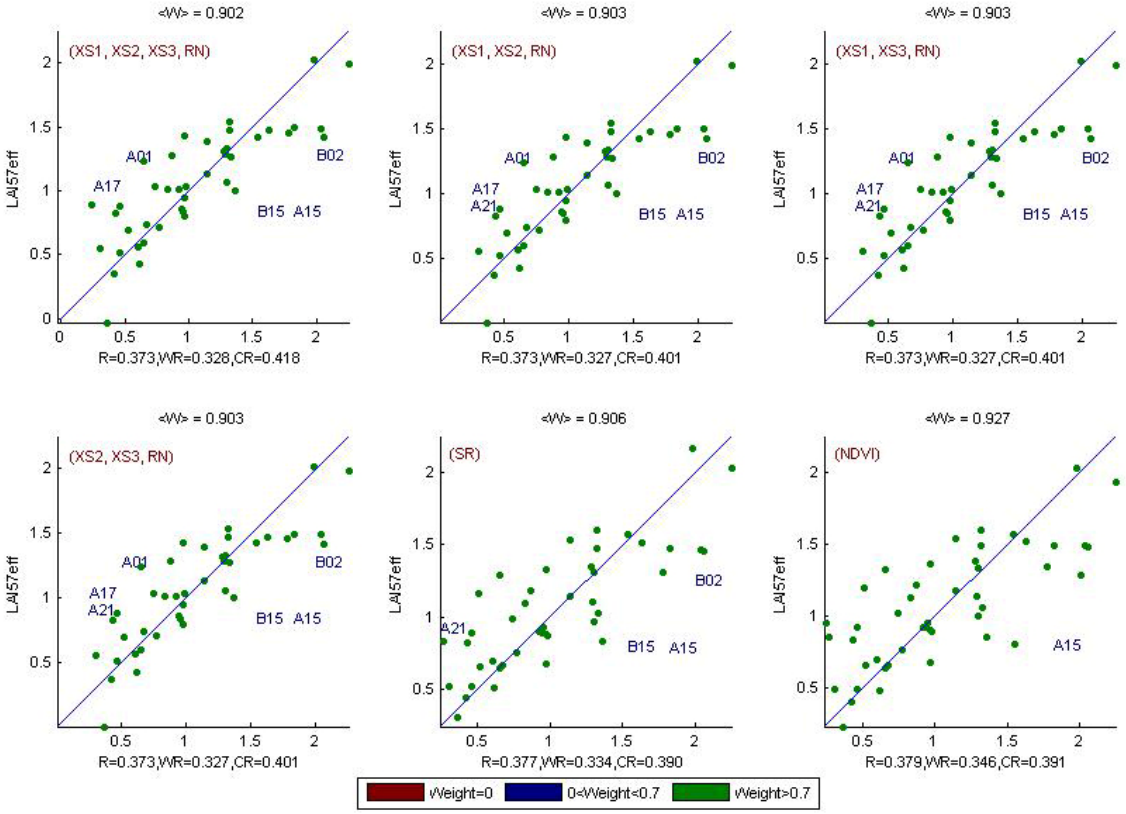

Figure 14. Effective LAI at 57.5°: results for regression on reflectance using different band combinations. R is the root mean square error computed between LAI57eff and estimated LAI57eff. WR is the weighted root mean square error and CR is the cross validation root mean square error.

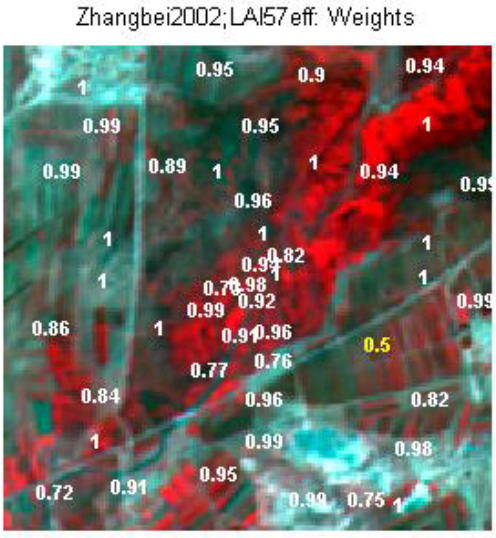

Figure 15. Weights associated to each ESU for the determination of LAI57eff transfer function.

For the LAI57true, the XS2, XS3, RN combination on reflectance (Figure 16 and Figure 17) was selected since it provides a good compromise between the cross-validation RMSE, the weighted RMSE (lowest value) and the RMSE (lowest value). Five weights are lower than 0.7.

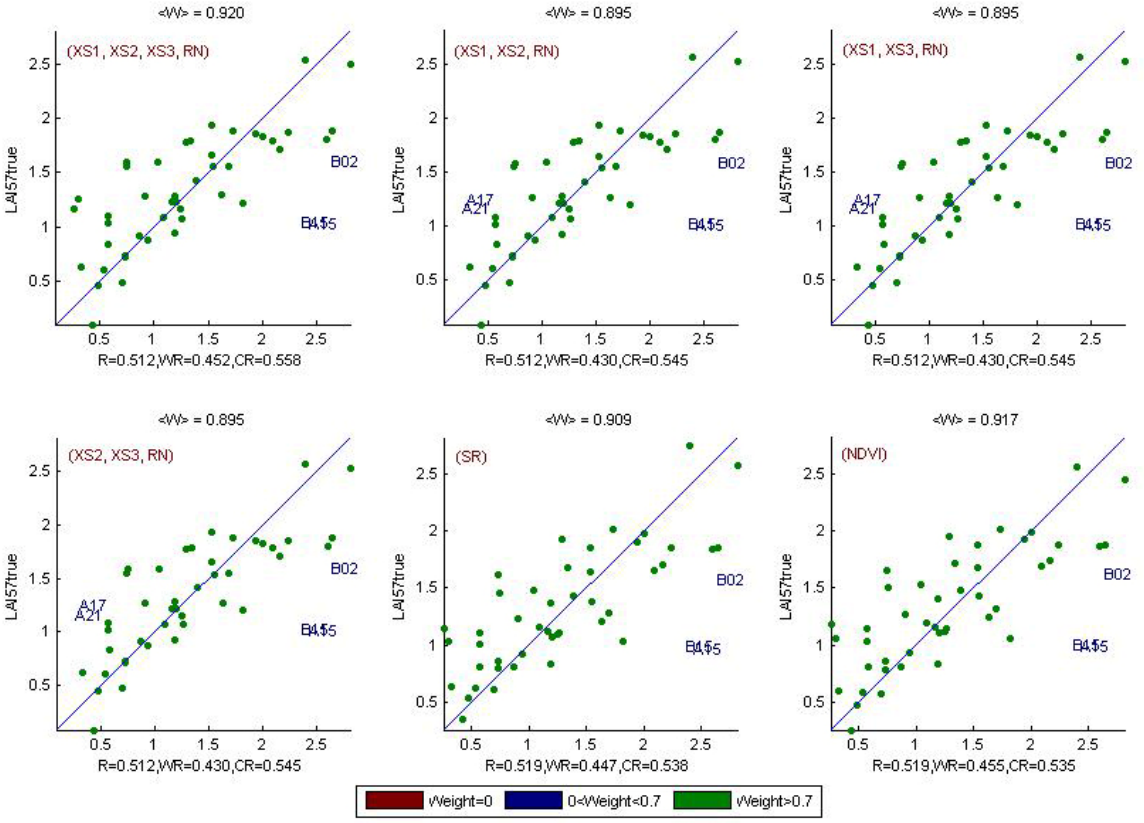

Figure 16. True Leaf Area Index at 57.5°: results for regression on reflectance using different band combinations. R is the root mean square error computed between LAI57true and estimated LAI57true. WR is the weighted root mean square error and CR is the cross validation root mean square error.

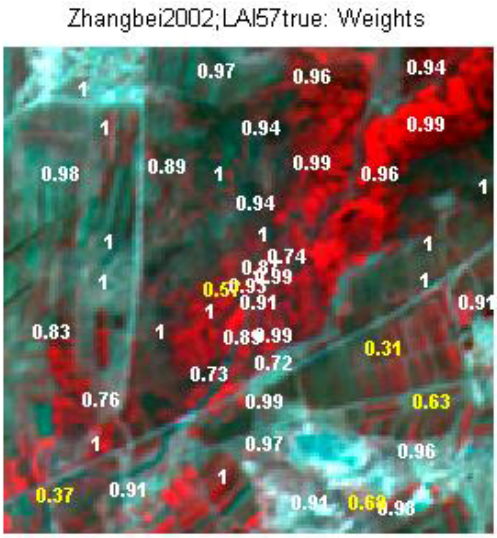

Figure 17. Weights associated to each ESU for the determination of LAI57true transfer function.

For the fCover, the XS1, XS2, XS3, RN combination on reflectance (Figure 18 and Figure 19) was selected since it provides a good compromise between the cross-validation RMSE, the weighted RMSE and the RMSE. Six weights are lower than 0.7.

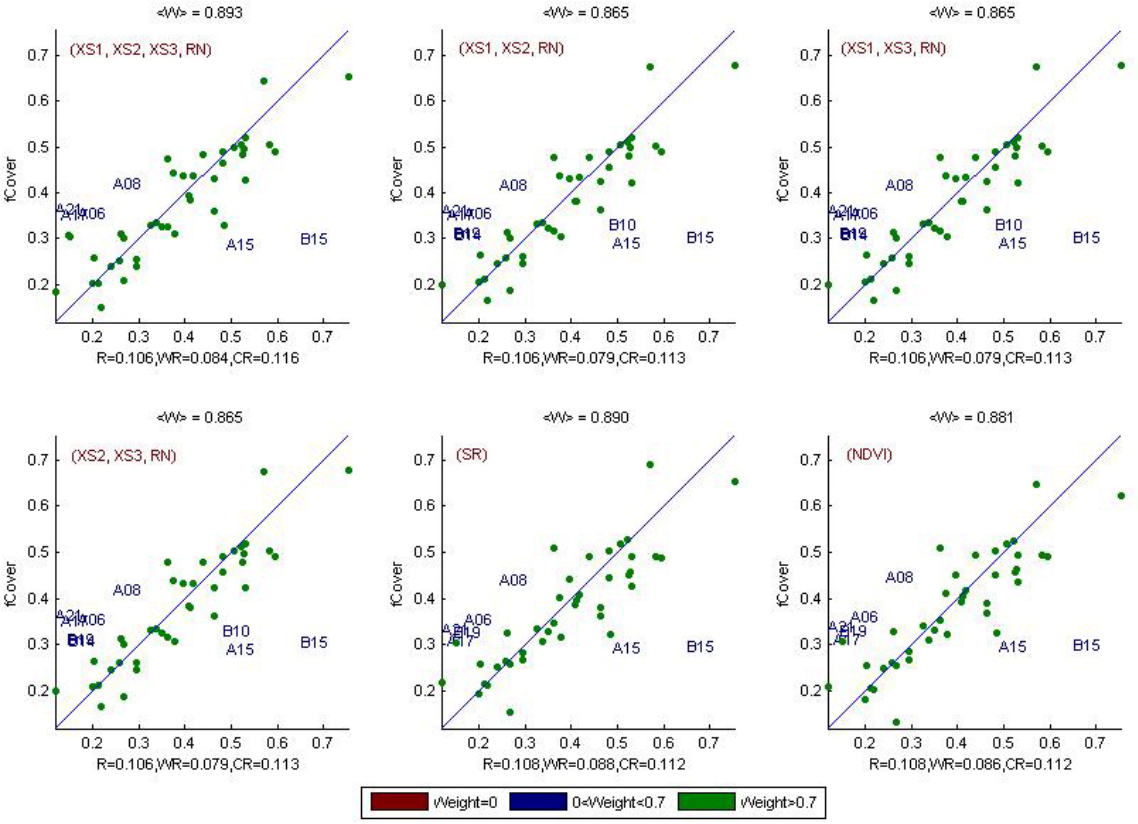

Figure 18. fCover: results for regression on reflectance using different band combinations. R is the root mean square error computed between fCover and estimated fCover. WR is the weighted root mean square error and CR is the cross validation root mean square error.

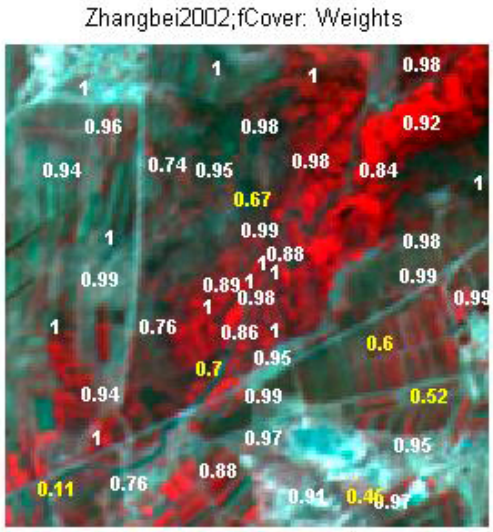

Figure 19. Weights associated to each ESU for the determination of fCover transfer function.

For the fAPAR, the NDVI combination on reflectance (Figure 20 and Figure 21) was selected since it provides a good compromise between the cross-validation RMSE, the RMSE and the number of weights are lower than 0.7 (six weights < 0.7).

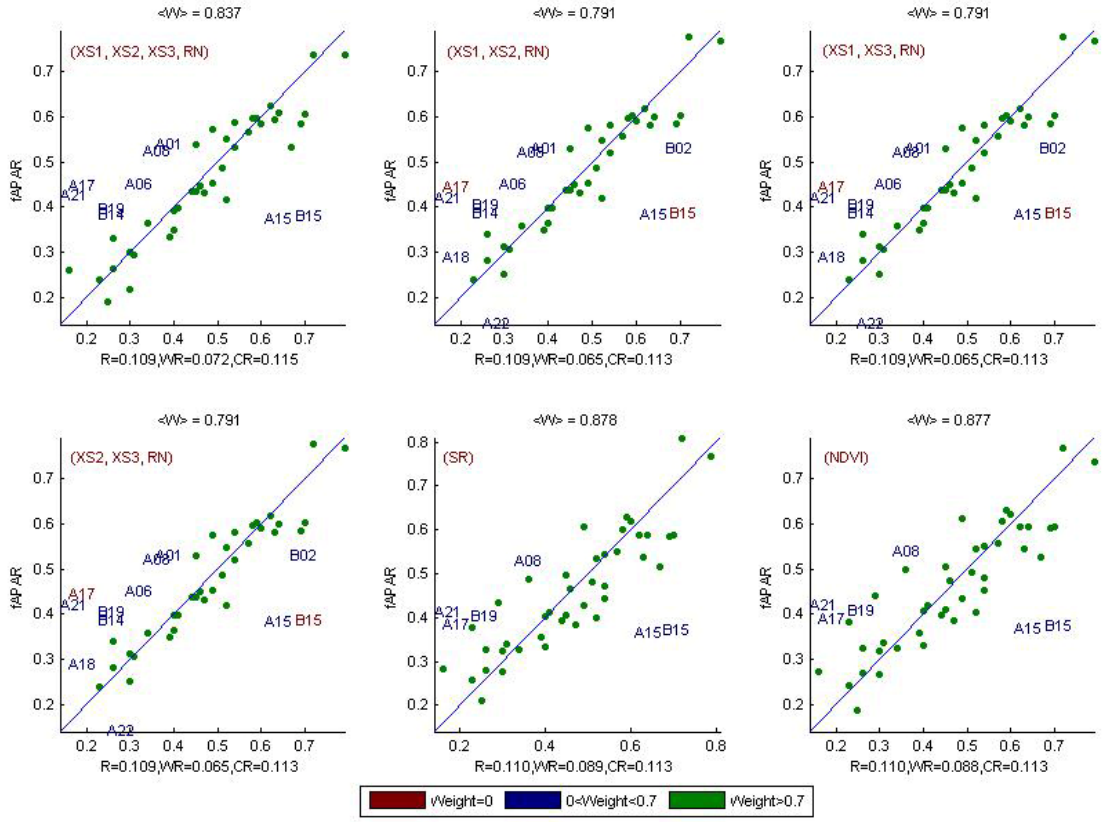

Figure 20. fAPAR: results for regression on reflectance using different band combinations. R is the root mean square error computed between fAPAR and estimated fAPAR. WR is the weighted root mean square error and CR is the cross validation root mean square error.

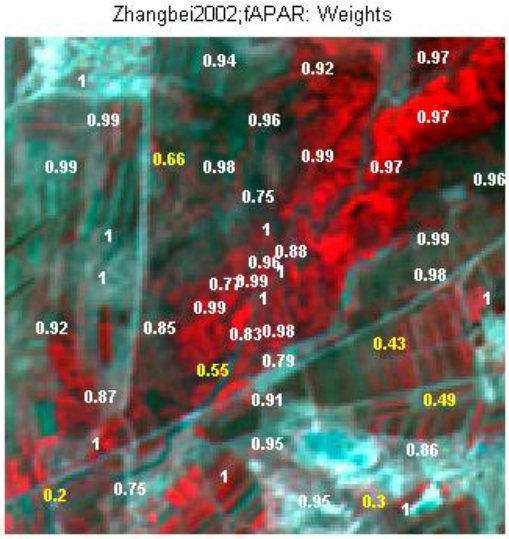

Figure 21. Weights associated to each ESU for the determination of fAPAR transfer function.

Following, the results of the transfer function (Table 2):

Variable	Band Combination	RMSE	Weighted RMSE	CR RMSE
LAIeff	5.5448 - 61.6635(XS2) - 7.2143(XS3) + 117.4205 (RN)	0.376	0.333	0.406
LAItrue	6.5054 - 70.8875(XS2) - 8.2349(XS3) + 131.7008(RN)	0.477	0.432	0.515
LAI57eff	-0.755 + 3.9456(NDVI)	0.379	0.346	0.391
LAI57true	5.7557 - 56.493(XS2) - 16.3207(XS3) + 130.0931(RN)	0.512	0.430	0.545
fCover	1.7333 -12.6553(XS1) - 10.7372(XS2) - 1.5794(XS3) + 58.5664(RN)	0.106	0.084	0.116
fAPAR	- 0.1323 + 1.2759(NDVI)	0.110	0.088	0.113

RN = Red*NIR

Table 2. Transfer function applied to the whole site for the different biophysical variables, and corresponding errors

3.3. Applying the transfer function to the Zhang Bei SPOT image extraction

Figure 22 presents the biophysical variable maps obtained with the transfer function described in Table 2 for all the classes. The maps obtained for the six variables are consistent, showing similar patterns: low LAIeff values where low fCover or fAPAR are observed and conversely… The difference between effective LAI and true LAI is significant (see the average values in Figure 22). This was expected when looking the LAIeff/LAItrue relationship, showing that for high LAI the difference between the two can be significant.

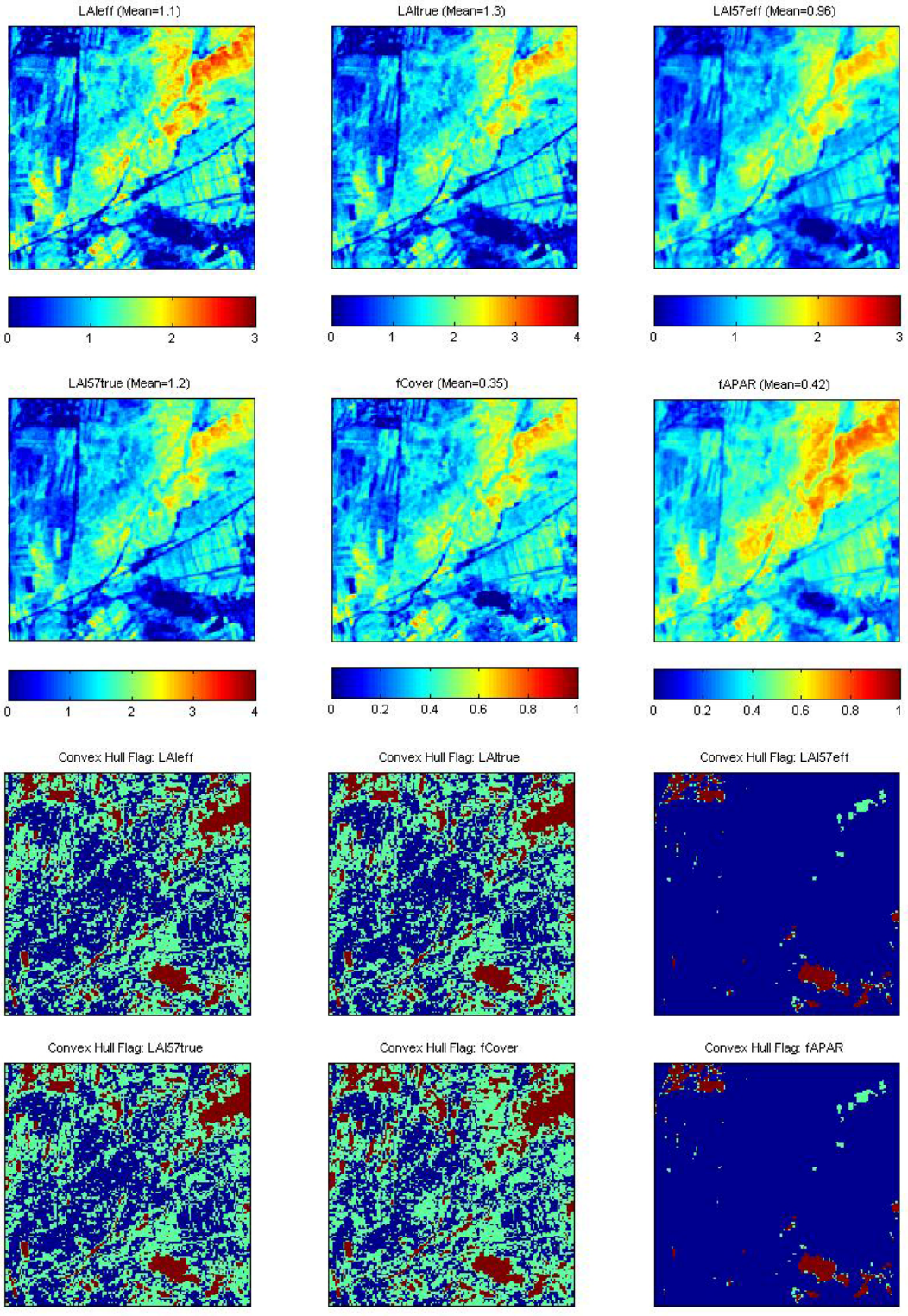

Figure 22. High resolution biophysical variable maps applied on the Zhang Bei site (top). Associated flags are shown: blue and light blue correspond to the pixels belonging to the 'strict' and 'large' convex hulls, red to the pixels for which the transfer function is extrapolating.

The extrapolation mainly corresponds to low NDVI values (<0.25: villages, bare soil…) and high NDVI values. Note that the flag maps are not comparable. For LAI57eff and fAPAR, the pixels inside the strict convex hull for are very numerous. This is due to the choice of the band combination. In theory, the more the number of bands increases, the larger the extrapolation is.

4. Conclusion

The 'REG' method is applied to all the classes by using 47 ESUs. The relationship between NDVI and LAI variables is consistent and the representativeness of the land cover of the different ESUs is good. The results of the robust regression are satisfactory. Note that the maps obtained for the biophysical variables are also consistent. The flag associated to each map shows that the extrapolation of the transfer function is mainly bounded to bare soil, high NDVI pixels… For all the variables, the regression coefficients are computed by relating the variable itself to reflectance.

The biophysical variable maps are available in UTM 50 North, WGS-84, projection coordinates at 20 m resolution.

5. Acknowledgements

We thank people who participated to the field experiment: **Denis Allard** (INRA, Biométrie, Avignon), **Xing-Fa Gu** (INRA, CSE, Avignon), **Yanli Anhui Qiao** (Institute of optics and Fine mechanics), **GU Yinqi Gu**, **Xianjun Min** (China Resource and Earth Satellite Data Application centre/CRESDA).

ANNEX

Ground measurement acquisition report for the VALERI site **Zhang Bei (China)**

sampled from 02/08/08 to 02/08/10

Marie Weiss, Denis Allard
Organization: INRA/NOVELTIS
email: denis.allard@avignon.inra.fr

Date of report: 20 May 2002

People participating to the field experiment:

Fistname & Name	**0rganization**
ALLARD Denis	INRA, Biométrie, Avignon
GU Xing-Fa	INRA, CSE, Avignon
QIAO Yanli	Anhui Institute of optics and Fine mechanics
GU Yinqi	China Resource and Earth Satellite Data Application centre (CRESDA)
MIN Xianjun	

Site coordinates

	Lat-Long WGS84 (Deg min.00)		UTM / WGS84 UTM 50N	
	Lat.	Long.	Easting	Northing
Upper left corner	41.29206653	114.66935576	304850	4573800
Lower right corner	41.26578446	114.70610264	307850	4570800

Ground control points

Name	Month	Day	Easting(m)	Northing(m)	Precision (m)	Comments on the vegetation status, condition of acquisitions, etc...
GCPA	8	10	303293	4569859	3	Crossing between main road and secondary one
GCPB	8	10	305526	4571294	3	1st crossing between secondary road and a dirt track towards the villages at the South East
GCPC	8	10	305595	4571327	3	2nd crossing between secondary road and a dirt track towards the villages at the South East
GCPD	8	10	305518	4571146	3	Crossing between dirt track and river
GCPE	8	10	305940	4571483	3	Crossing between secondary road and river
GCPF	8	10	307673	4572441	2	Crossing between secondary road and a dirt track towards the villages at the South East

Description of the site and land cover

Category according to IGBP classification

Grassland.

Comments on the land cover

The area is composed of plateau (1400 m) with pastures (for sheeps and cows) and little crops that are generally located near the villages. There are many small villages, separated from 2 to 4kms. It was therefore not easy to find a 3kmx3km area really homogeneous without villages.
The region was chosen as it was quite homogeneous, accessible from the road, and presented no woody part. The centre is composed of pastures (high and low vegetation). In the NE, SE, and SW corners, there are 3 small villages with crops at the South. Some crops have been sampled but the plots are sometimes so small that a "VALERI" cross stretched on 2 plots.

Topography

Altitude ~1400m

Spatial Sampling scheme

Sensors used for sampling the ESUs

	Method	**Comments**
☒	Hemispherical photographs	47 crosses have been measured, most of them by acquiring 12 images. The VALERI area center was over sampled (13 ESUs).
☐	LAI2000	
☐	TRAC	
☐	Ceptometer	
☐	Direct measurements	
☐	Other	

Sampling strategy for the ESU

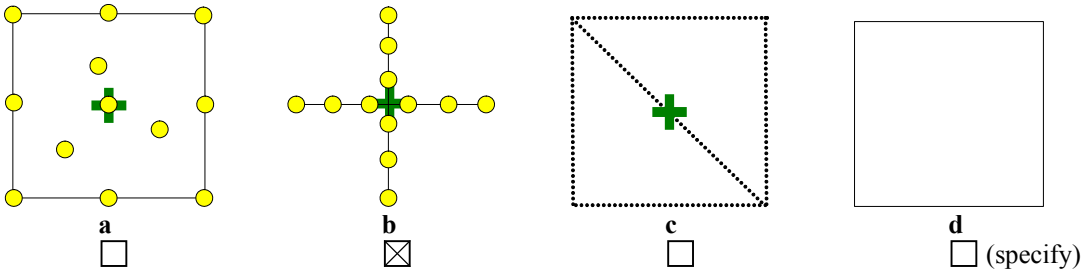

a ☐ **b** ☒ **c** ☐ **d** ☐ (specify)

Distribution of the Elementary sampling units

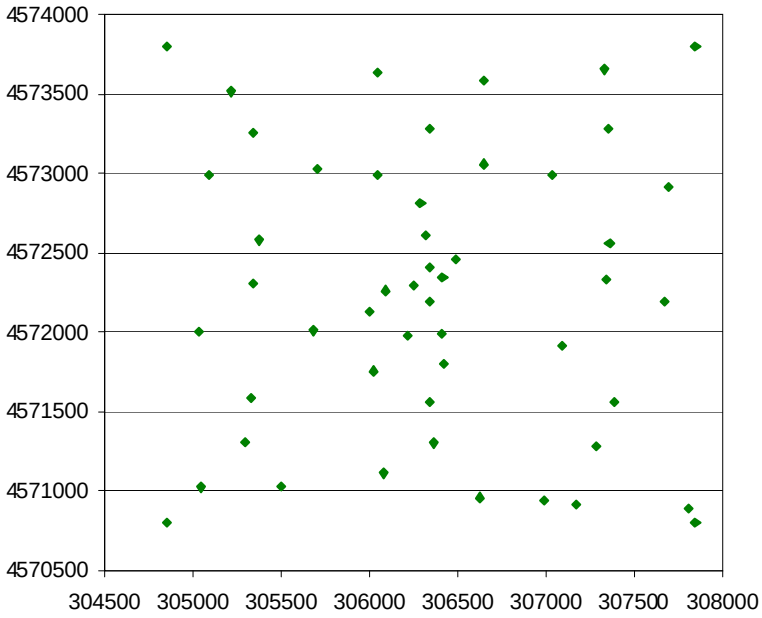

The high spatial resolution image

Satellite

Satellite used	SPOT2 HRV1
Level of processing	1A
Projection type	UTM 50 North, WGS-84
Acquisition date	2002/08/23

List of the ESUs

A01	A	8	8	306422	4571803	5	11 images, grassland
A02	A	8	8	306408	4571993	6	12 images, grassland, no visible horizon
A03	A	8	8	306344	4572191	5	12 images, grassland, no visible horizon, near the river
A04	A	8	8	306343	4572401	6	12 images, grassland
A05	A	8	8	306325	4572611	6	12 images, grassland
A06	A	8	8	306292	4572808	5	12 images, grassland
A07	A	8	8	306223	4571976	4	12 images, grassland
A08	A	8	8	306021	4571753	4	12 images, grassland
A09	A	8	9	307333	4573652	4	12 images, grassland
A10	A	8	9	307351	4573284	4	12 images, grassland
A11	A	8	9	307698	4572909	4	11 images, grassland
A12	A	8	9	307041	4572985	5	12 images, grassland
A13	A	8	9	307361	4572558	5	12 images, low grassland
A14	A	8	9	307340	4572328	5	12 images, low grassland
A15	A	8	9	307096	4571910	5	12 images, Truck farming, very small fields
A16	A	8	9	307671	4572187	4	12 images, Truck farming, very small fields
A17	A	8	9	307388	4571559	4	12 images, low grassland
A18	A	8	9	307289	4571276	4	12 images, low grassland
A19	A	8	9	307807	4570892	4	12 images, low grassland
A20	A	8	9	307170	4570909	5	12 images, Truck farming, very small fields + woods
A21	A	8	9	306992	4570942	5	12 images, low grassland
A22	A	8	9	306629	4570957	5	12 images, low grassland…sheeps
A23	A	8	9	306083	4571109	5	12 images, grren vegetable (turnip?)
A24	A	8	9	306362	4571299	5	12 images, low grassland
A25	A	8	10	306047	4572986	4	12 images, grassland
A26	A	8	10	306052	4573631	4	12 images, Truck farming, very small fields near grasland
A27	A	8	10	306648	4573584	4	12 images, grassland
A28	A	8	10	306340	4573276	4	12 images, grassland
A29	A	8	10	306648	4573057	4	12 images, grassland
B01	B	8	8	306258	4572289	5	13 images, grassland
B02	B	8	8	306097	4572261	6	12 images, grassland
B03	B	8	8	306000	4572126	6	12 images, grassland
B04	B	8	8	306416	4572343	6	12 images, grassland
B05	B	8	8	306489	4572461	6	12 images, grassland
B10	B	8	9	305687	4572008	5	12 images, low grassland
B11	B	8	9	305340	4572306	5	12 images, low grassland
B12	B	8	9	305378	4572577	5	12 images, low grassland
B13	B	8	9	305037	4572001	5	12 images, Truck farming, very small fields (kind of wheat)
B14	B	8	9	305507	4571023	5	12 images, low grassland close to a village
B15	B	8	9	305052	4571021	5	12 images, vegetable
B16	B	8	9	305295	4571308	5	12 images, low grassland
B17	B	8	9	305331	4571586	5	12 images, grassland
B18	B	8	9	306346	4571562	5	12 images, grassland
B19	B	8	10	305709	4573021	4	12 images, low grassland
B20	B	8	10	305344	4573259	4	12 images, low grassland
B21	B	8	10	305222	4573513	4	12 images, low grassland
B22	B	8	10	305089	4572992	4	12 images, grassland